Materials and Design 195 (2020) 108997

Contents lists available at ScienceDirect

Materials and Design

journal homepage: www.elsevier.com/locate/matdes

Mechanism of twist in incremental sheet forming of thermoplastic polymer

Zhiyun Yang, Fei Chen *

National Engineering Research Center of Die and Mold CAD, Shanghai Jiao Tong University, 1954 Huashan Road, Shanghai 200030, PR China

HIGHLIGHTS

- The twist mechanism was revealed by experimental and theoretical analysis.
- A new analytical model to calculate the twist angle was derived and verified.
- A novel alternate spiral tool trajectory was established.
- The twist defect was effectually restrained.
- The wrinkle defect was completely eliminated.

GRAPHICAL ABSTRACT

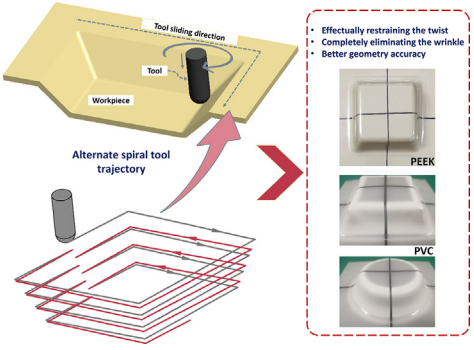

ARTICLE INFO

Article history:
Received 28 June 2020
Received in revised form 21 July 2020
Accepted 24 July 2020
Available online 1 August 2020

Keywords:
Incremental sheet forming
Twist
Thermoplastic polymer

ABSTRACT

Single point incremental forming (SPIF) is one of the procedures with the most potential in aerospace development and human implants. However, twist phenomena occur frequently and affect the processing defects, which strongly influence the geometric accuracy of the formed parts. This work reveals the mechanism of twist phenomena in detail and figures out the optimal solution of the principal challenge during industrial application and artificial bone processing by SPIF. A new analytical model is proposed to calculate the twist angle based on the law of conservation of energy. Meanwhile, a novel alternate spiral tool trajectory is established according to the linear interpolation of the two adjacent contour lines. Based on the case studies including pyramid frustum shape with constant wall angle and truncated cone shape with varying wall angle, SPIF formed parts by using the alternate spiral trajectory are compared with that by traditional unidirectional spiral trajectory, to effectively understand the advantages of the developed tool trajectory strategy. It shows that the proposed alternate spiral trajectory provides an effective way to effectually restrain the twist, and finally improves the geometric accuracy of target part in practical application of SPIF.

1. Introduction

Flexible and rapid methods of manufacturing high strength but lightweight polymeric parts have become more widespread in aerospace development and human implants. As a method of low-cost, small-batch and flexible forming of sheets without mold [1], single point incremental forming (SPIF) has been utilized to fabricate the polymeric sheet parts within the past years [2].

Franzen et al. [3] made a creative study in the experimental investigation on forming sheet parts made of polyvinylchloride (PVC) in terms of the conical parts with a continuously increasing wall angle. Martins et al. [4] greatly extended the application scope of SPIF technology to five thermoplastic materials, in which three failure models (circumferential crack, twist and oblique crack) were systematically summarized for the first time. It was also found even at room temperature SPIF has

* Corresponding author.
E-mail address: feichen@sjtu.edu.cn (F. Chen).

https://doi.org/10.1016/j.matdes.2020.108997

potential for manufacturing of complex polymeric parts with very high depths. Another important breakthrough which Silva et al. [5] put forward is the theoretical explanation of new failure modes by using membrane analysis method inaugurated by Silva et al. [6]. Aiming to identify the key influential operative variables in the SPIF of polymers and further to determine the effects of polymeric material structures varying from high crystalline to amorphous on the formability limits, Marques et al.[7] evaluated the full potential of SPIF in rapid prototyping polymer sheet parts in which experiment tests and membrane analysis were combined. As a result of continuous effort in the SPIF development, polymeric sheet parts with varying wall angle conical frusta and pyramid frusta could be quickly formed using simple generic tools by developing geometry-specific tool paths. However, there are still some challenges left that need to be fixed first before extensive industrial applications, in which the most critical is the geometric deviation induced by the twist in SPIF of the polymeric sheet parts.

As an undesired failure mode, twist phenomena have been observed by many researchers in SPIF of polymeric sheet as well as metal sheet. Matsubara et al. [8] demonstrated that twist phenomenon was uncontrollable. The main reason could be attributed to the sample that has already been formed is compelled to rotate around the fixed tool by movements of the forming tool. Jeswiet et al. [9] further proposed that the tensile defects on surface of formed part was caused by tool trajectory with constant height and the unidirectional trajectory. The study by Vanhove et al. [10] launched an in-depth analysis of twist phenomenon which can be divided into two categories: forward twist and reverse twist. At lower drawing angles, forward twist plays the key role due to the monotonous tangential force component exerted on the workpiece when using unidirectional toolpaths. At relatively high drawing angles, the reverse twist becomes dominant along with the enhancement of the asymmetric strain, asymmetric thickness and force distribution. Duflou et al. [11] provided a more detailed information by means of strain measurement and FEA simulations, explained the underlying causes of twist phenomena in SPIF of metal sheet, arrived at a conclusion that the combination of continued strain accumulation and asymmetric stress levels dominates the twist phenomena at high drawing angles.

Based on the above experimental results and theoretical analysis, some researchers began to engage in tool path strategy optimization to further eliminate twist defects in SPIF. Dejardin et al. [12] developed a new tool path strategy in terms of changing the direction of movement of the forming tool in each contour line. Recently, Durante et al. [13] also developed a novel alternate spiral toolpath (ATP) to eliminate twist defects on the wall of the manufactured polycarbonate (PC) sheets with 1.9 mm initial thickness. Chang and Chen [14] proposed an analytical model of twist angle for SPIF of metal sheet. It was found that the torque generated by the uneven distribution of the circumferential friction stress along the meridianal direction plays the dominant role in the twist phenomenon. Meanwhile, a strikingly similar conclusion that twist direction mainly depends on the derivative of through-thickness stress to wall angle has been yielded. The effect of twist on geometric accuracy could be reduced by selected appropriate process parameters. Based on our latest research [15], it was found that twist is a common phenomenon in hot incremental forming of polyether-ether-ketone (PEEK) due to the unidirectional tool path strategy and material flow. By comparing the existing experimental results, it can be concluded that the twist phenomenon does not significantly affect the formed shape of metal parts except in some applications [16]. However, as for polymer, especially under the condition of Joule heating, the twist angle is up to 20°, which affects the accuracy and geometrical shape of formed parts greatly and even causes severe wrinkle defects along the inclined wall of the formed parts.

In summary, according to previous experimental studies by Martins et al. [17], it is commonly recognized that SPIF can give the successful manufacture of polymeric sheet parts such as PVC, PC, POM, PA, with large drawing angles and forming depths even at room temperature. But our previous study has fully testified that not all thermoplastics have good formability at room temperature. Aiming to increase polymer formability, a special experimental setup was designed and built to characterize the thermal formability of PEEK by using SPIF. The results of experiments show that hot incremental sheet forming can greatly reduce the traditional defects including circumferential crack and oblique crack in SPIF of polymer when the heating temperature is close to the glass transition temperature of polymer. But this forming mode cannot eliminate the twist phenomena due to the polymer formed in a high elastic state. Therefore, how to achieve a high part accuracy without twist is a new challenge in promoting SPIF of thermoplastics.

This study attempts to further reveal the twist mechanism in hot incremental forming of thermoplastic polymer by means of a combined theoretical and experimental investigations. A new analytical model was proposed to predict the twist angle. Section 2 particularly introduces the reasons why the twist phenomena are inevitable by using unidirectional trajectory. In order to eliminate the twist defects, a novel continuous alternate spiral trajectory algorithm was developed and carried out in Section 3. In Section 4, to verify the general applicability of the tool trajectory, this algorithm was further extended to form PVC. Meanwhile, detail discussions are included in Sections 3 and 4, followed by the conclusions in Section 5.

2. Analysis of twist mechanism

2.1. SPIF of PEEK experiments

As reported by Chen et al. [18], Poly-ether-ether-ketone (PEEK) is an engineering thermoplastic with high tensile strength and good biocompatibility. Beyond this, McLauchlin et al. [19] found that excellent chemical stability and reprocessability of PEEK make it possible to use in the space manufacturing to reduce the need of raw materials. In this study, PEEK sheet with the size of 1000 mm × 660 mm × 3 mm was provided by Junhua Company. The polymer sheet was cut into square plates with a size of 150 mm × 150 mm by a shearing machine. The glass transition temperature of PEEK is 143°C. Table 1 gives the mechanical and thermal properties of the material. The process parameters are as follows: the step depth of 0.4 mm, tool diameter of 10 mm, tool rotation speed of 100 r/min and Grease MP-3 continuous lubrication. To ensure a better formability, the forming temperature was maintained at 100 °C. Fig.1 shows the schematic diagram of the thermal assisted incremental forming experimental setup. The final twist angle was measured by the center cross line on the outer surface of formed part.

Fig. 2(a) shows the truncated funnel parts with varying angle from 60° to 90°. The forming parameters are as follows: the diameter of 60mm and forming depth of 30mm. It can be seen that significant twist phenomenon occurs along the tool sliding direction. Especially, with the increase of depth and forming angle, the twist phenomenon becomes more obvious. To further explore the influence of geometry and wall angle on twist phenomena, detailed experiments were carried out. The target shapes are pyramid parts with constant wall angles of 45°, 60° and 70°, respectively. As shown in Fig. 2(b), (c) and (d), the twist angle also increases with the increase of the wall angle.

According to experimental results, twist phenomena in hot SPIF of polymer are mainly due to the continuous unidirectional movement of the tool. It can be concluded:

Table 1
Material properties of PEEK.

Mechanical properties		Thermal properties	
Elastic modulus (GPa)	3.6	Thermal conductivity (W/mk)	4.7
Density (kg/m^3)	1300	Specific heat (J/kg K)	2180
Poisso's ratio	0.38	Glass transition temperature(K)	416
Yield stress (MPa)	107	Melting temperature(K)	616

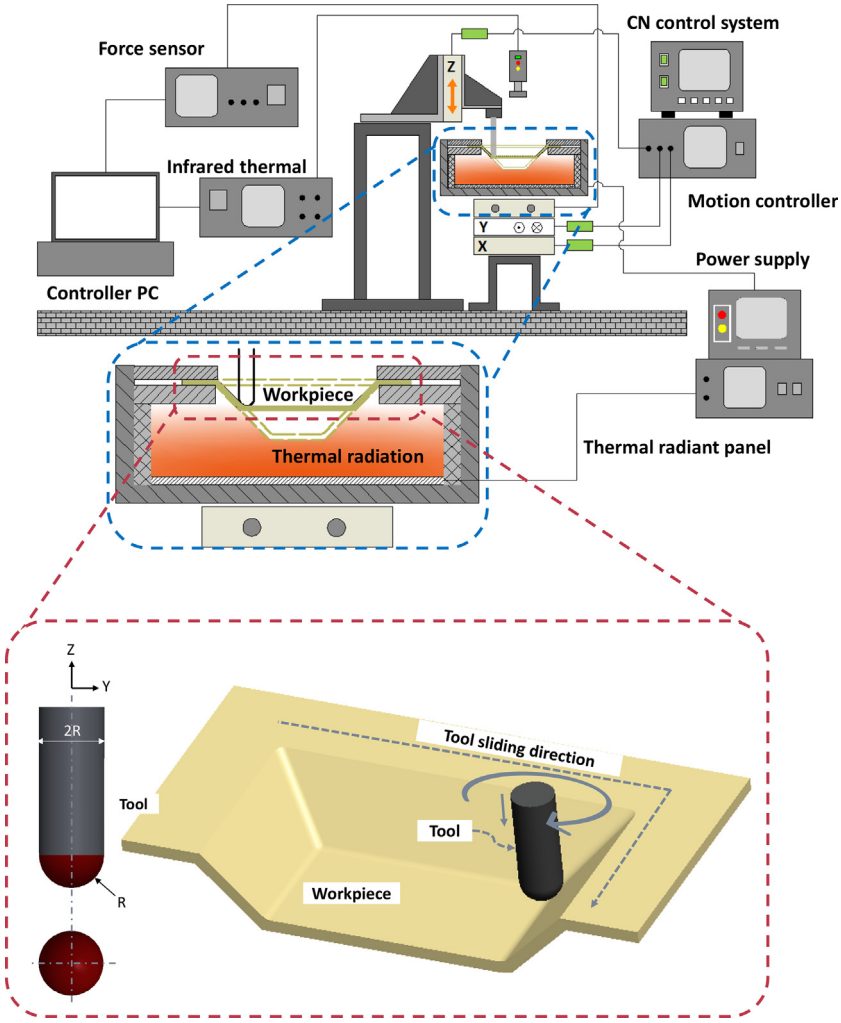

Fig. 1. Experimental setup for thermal assisted single point incremental forming.

(1) With the increase of the forming angle, the contact zone between tool and polymer sheet becomes larger, resulting in more materials pushed along the tool sliding direction. The flow and accumulation of materials along the unidirectional tool movement eventually leads to the twist of the formed part.
(2) Due to the friction caused by the through thickness stress of contact zone between tool and sheet, the shear strain of polymer sheet in contact zone along the tool sliding direction is accumulated.

2.2. Analysis of the twist mechanism

In this section, the causes of twist phenomena in the heat-assisted SPIF of polymer sheet are analyzed from two aspects. On the one hand, the contact area between polymer sheet and tool in the tool sliding direction is calculated. On the other hand, the contact stress along the thickness direction is calculated, and shear strain and shear stress along the tool sliding direction caused by friction is also analyzed. Finally, an analytical model of twist angel is proposed.

2.2.1. Calculation of the contact area

In SPIF process of polymer, the calculation of contact area between tool head and polymer sheet is an important factor to control material flow. Asghar et al. [20] assumed that the indentation produced by sliding of tool head between inclined wall and bottom surface is called the contact zone. As shown in Fig. 3, the expression of contact zone is obtained by observing in CAD model. Li et al.[21] innovatively update the calculation method of the contact area through parameter optimization and predicted the force in the process of single point incremental forming. Liu et al.[22] optimized the calculation method of contact area by observing the actual contact conditions and considering the influence of all parameters on the contact area.

In the process of incremental forming, neglecting the effects of undeformed polymer sheet bending, the tool head moves along the forming trajectory, maintaining a constant indentation. In the work, the main purpose is to study the influence of unidirectional trajectory on twist, so only the contact zone between tool head and polymer sheet in the circumferential direction was considered, which is mainly determined by the following two parts: $\Phi 1$ below the plane of undeformed sheet and $\Phi 2$ above the plane of undeformed sheet (Fig. 4b).

The contact zone of circumferential direction between tool head and polymer sheet was calculated in terms of tool radius$r$, step depth ΔZ and central angle δ as,

$$\Phi_1 = \frac{2\delta\pi r^2}{360} - \frac{1}{2}\times 2\left\langle\sqrt{r^2-(r-f_Z)^2}\right\rangle(r-f_Z) \tag{1}$$

$$\Phi_2 = \frac{\gamma\pi r^2}{360} - \frac{1}{2}\times 2\left\langle\sqrt{r^2-(r-f'_z)^2}\right\rangle(r-f'_z) \tag{2}$$

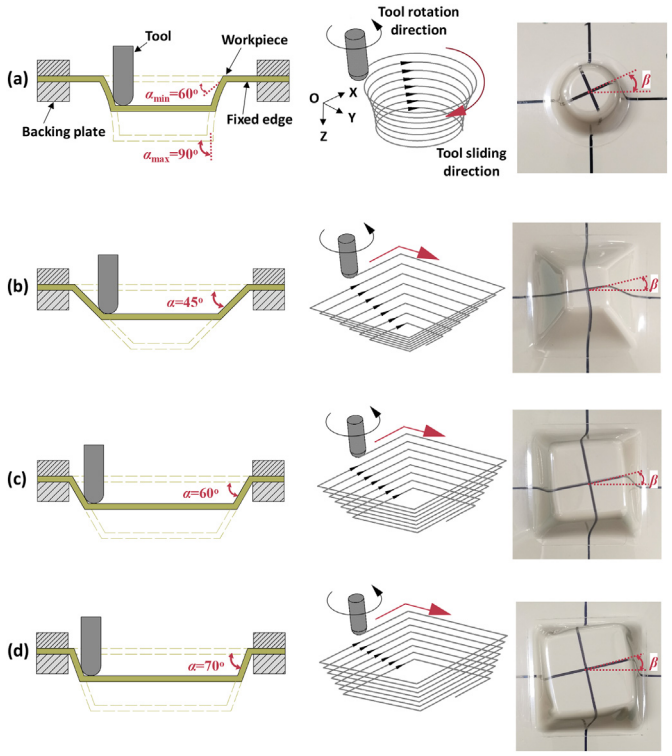

Fig. 2. The formed parts of PEEK by unidirectional toolpath. (a) The truncated cone with varying wall angle α from 60° to 90° and truncated pyramid with the constant wall angles of (b) 45°, (c) 60° and (d) 70°, respectively. The measured twist angles are 22°, 6 °, 10 ° and 15 °, respectively.

As shown in Fig. 3(b), 2δ is the center angle corresponding to the blue region, $\delta = \cos^{-1}(1 - f_z/r)$. γ is the center angle corresponding to the green region, which is not only related to δ, but also to the wall angle of the target part,$\gamma = \int_{\delta}^{\alpha} d\gamma$, $\alpha$is the wall angle of part. As shown in Fig. 3(c), f_Z is the unit incremental depth corresponding to the tool moving one revolution along the unidirectional spiral trajectory, $f_Z = \Delta Z/L$, L is the circumference corresponding to the tool moving one revolution along the trajectory. $f_Z^{'}$ is the height corresponding to the green region, which is determined by the scallop height of polymer sheet formed surface, and $f_Z^{'} \approx s$.

From Eqs. (1) and (2), an analytical expression for estimating the contact area of Φ can be written as,

$$\Phi = \Phi_1 + \Phi_2 = \frac{\langle \cos^{-1}(1-f_Z/r)+\alpha \rangle \pi r^2}{360} - \left(\sqrt{r^2-(r-\Delta Z/L)^2}\right)(r-\Delta Z/L) - \frac{\Delta Z}{2\sin\alpha}\sqrt{r^2-\left(\frac{\Delta Z}{2\sin\alpha}\right)^2} \quad (3)$$

It is evident from the Eq. (3) that the contact area is related to the tool diameter, wall angle and step depth. As shown in Fig. 4, contact area increases with the increase of tool diameter and wall angle, but decreases with the increase of step down. This phenomenon may be due to the increase of step down, which enhances the tensile effect of polymer sheet along the meridional direction, so reduces the contact area in circumferential direction. In this work, tool diameter and step down are constants, with the increase of wall angle α, the contact area also increases, and more materials of side wall is pushed by tool along the sliding direction, which may be able to provide some explanations of the change in Fig. 2. It is obvious that as the forming angle increases, the twist of formed part becomes more and more severe. The materials flow in contact zone along tool sliding direction also affects the

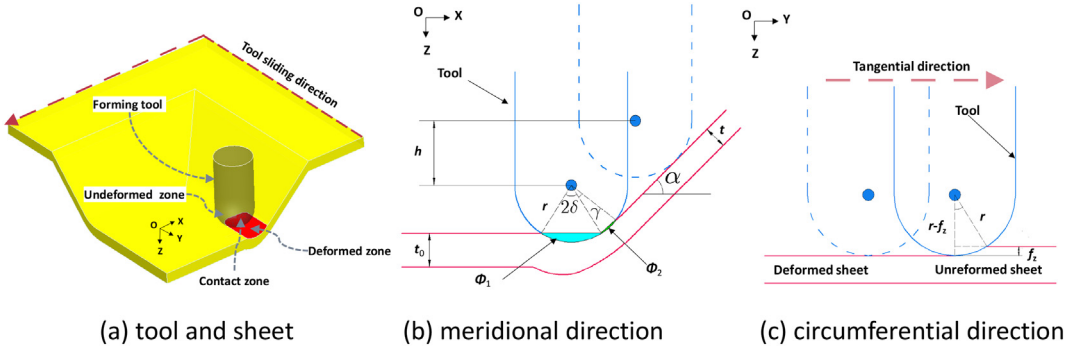

Fig. 3. Schematic of the indentation by the tool head sliding on a flat surface.

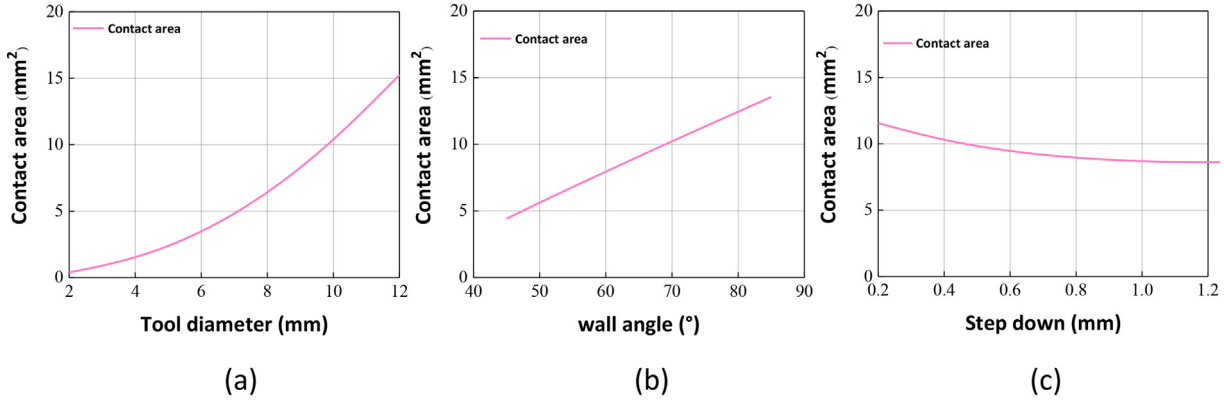

Fig. 4. Influence of process parameters of (a) step depth, (b) wall angle and (c) tool diameter on the scallop height.

symmetrical distribution of wall thickness in circumferential direction, which will be verified by relevant experiments in Section 2.2.4.

2.2.2. Membrane equilibrium analysis

Silva et al. [6] did a path breaking study on the analytical modelling of the contact stress state based on membrane analysis. This model was applied in this section. Chang et al. [23] adopted this model to predict the forming force of several typical incremental forming. Jackson et al. [24] measured the thickness deformation mechanism of copper truncated cone sheet, and further verified the effects of shear force parallel and perpendicular to tool sliding direction on the deformation mechanism of single point incremental forming. As shown in Fig. 5(b), the stress component of the small element in the contact zone determines the shear stress in tool sliding direction.

As Silva et al. [6] mentioned, the simplified assumptions were made as follows:

(1) Neglecting the effects of bending and strain hardening during incremental forming;
(2) Assuming that the material is isotropic;
(3) The friction stress exerted at the tool–sheet contact interface is assumed to be made of two components in terms of circumferential direction component $\mu_\theta\sigma_t$ due to circumference movement of the tool and meridional direction component $\mu_\varphi\sigma_t$ due to the step down movement of the tool.

According to the membrane analysis, along the circumferential direction, the force equilibrium equation can be expressed as,

$$\sigma_\theta r d\alpha\left(t+\frac{\mathrm{dt}}{2}\right)-\mu_\theta\sigma_t r d\alpha\left(r+\frac{dr}{2}\right)d\theta-(\sigma_\theta+d\sigma_\theta)rd\alpha\left(t+\frac{dt}{2}\right)=0 \quad (4)$$

Along the thickness direction, the force equilibrium equation can be expressed as,

$$\sigma_t r_1 d\theta r d\alpha+\sigma_\varphi r_1 d\theta t\,\sin\frac{d\alpha}{2}+(\sigma_\varphi+d\sigma_\varphi)(r_1+dr_1)d\theta(t+dt)\,\sin\frac{d\alpha}{2}$$
$$+\sigma_\theta r d\alpha t\,\sin\frac{d\theta}{2}\,\cos\alpha+(\sigma_\theta+d\sigma_\theta)rd\alpha t\,\sin\frac{d\theta}{2}\,\cos\alpha=0 \quad (5)$$

Along the meridional direction, the force equilibrium equation can be expressed as,

$$(\sigma_\varphi+d\sigma_\varphi)(r_1+dr_1)d\theta(t+dt)-\sigma_\varphi r_1 d\theta t+\mu_\varphi\sigma_t r_1 d\theta r d\alpha$$
$$-\sigma_\theta\,\sin\frac{d\theta}{2}rd\alpha t\,\sin\alpha-(\sigma_\theta+d\sigma_\theta)\,\sin\frac{d\theta}{2}rd\alpha t\,\sin\alpha=0 \quad (6)$$

And the friction conditions can be expressed as,

$$\tau_\theta=\mu_\theta\sigma_t \quad (7)$$

$$\tau_\varphi=\mu_\varphi\sigma_t \quad (8)$$

where μ_θ is the friction coefficient between tool and polymer sheet in circumferential direction, and $\mu_\varphi$is the friction coefficient between tool and polymer sheet in meridional direction, the coefficient of friction can be calculated as:

$$\mu=\sqrt{\mu_\theta^2+\mu_\varphi^2} \quad (9)$$

After neglecting higher-order terms and simplifying the above equations, Eq. (4) can be simplified as:

$$d\sigma_\theta=-\mu_\theta\sigma_t\frac{rd\theta}{t}\cong-\mu_\theta\sigma_t \quad (10)$$

Taking into account that $r_1=r_2\cos\alpha$ and Eq. (5) can be simplified as:

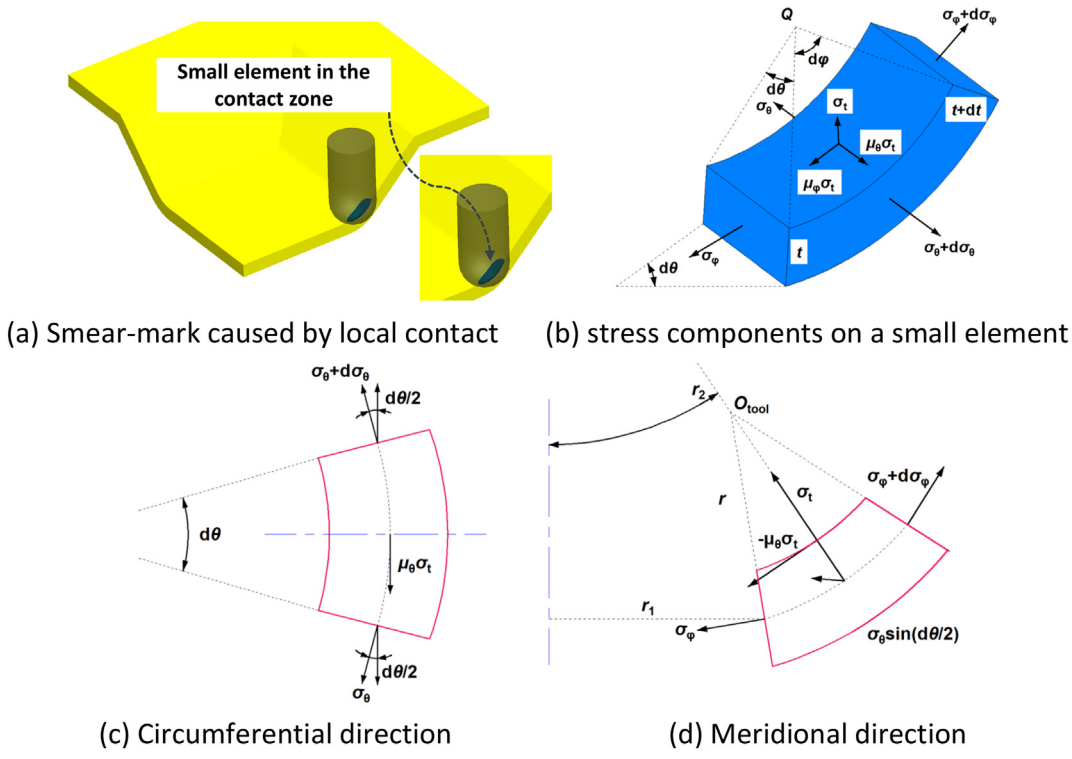

Fig. 5. Contact stress of small element.

$$\frac{\sigma_t}{t}+\frac{2\sigma_\phi}{r}+\frac{2\sigma_\theta}{r_2}=0 \tag{11}$$

further:

$$\sigma_t=-\frac{2t\sigma_\phi}{r}-\frac{2t\sigma_\theta}{r_2} \tag{12}$$

By considering the Levy-Mises constitutive equation in plane strain condition ($d\varepsilon_\theta=0$), as follow:

$$\sigma_\theta=\frac{1}{2}(\sigma_t+\sigma_\varphi) \tag{13}$$

and

$$\begin{cases}\sigma_\varphi=\sigma_1\\ \sigma_\theta=\sigma_2\\ \sigma_t=\sigma_3\end{cases} \tag{14}$$

Equivalent stress can be calculated as follow:

$$\overline{\sigma}=\frac{1}{\sqrt{2}}\sqrt{(\sigma_1-\sigma_2)^2+(\sigma_2-\sigma_3)^2+(\sigma_3-\sigma_1)^2} \tag{15}$$

Based on the above equations, the through-thickness stress can be represented as:

$$\sigma_t=-\frac{4t}{\sqrt{3}r+2\sqrt{3}t}\overline{\sigma} \tag{16}$$

where $\overline{\sigma}$ is the equivalent stress, which can be calculated by following flow stress model, while A is the yield stress, B is the strain hardening coefficient, n is the hardening exponent.

$$\overline{\sigma}=A+B\overline{\varepsilon}^n \tag{17}$$

Based on the volume constancy assumption and plane strain state, combined with cosine law with thickness variation, the calculation method of equivalent plastic strain is as follows:

$$\overline{\varepsilon}=\frac{\sqrt{2}}{3}\sqrt{(\varepsilon_\varphi-\varepsilon_\theta)^2+(\varepsilon_t-\varepsilon_\theta)^2+(\varepsilon_t-\varepsilon_\varphi)^2}=\frac{\sqrt{2}}{3}\ln\frac{1}{\cos\alpha} \tag{18}$$

As shown in Fig. 6, the through thickness stress results in the strain ε_{22} and shear strain γ_{21} along the thickness direction in the (1, 2) plane, and the friction shear stress along the tool sliding direction causes shear strain γ_{31} in the (1, 3) plane. The strain along thickness direction can be measured by thickness of formed part, and the thickness of formed part conforms to cosine law. The strain along tool sliding direction can be measured by the surface grid element.

2.2.3. Analytical modeling for twist angle

According to the above analysis, the mechanisms of the twist phenomena are as follows: the material flow in the local contact zone of polymer sheet caused by the sliding of the tool, and the through-thickness stress distribution under the tool head leads to the circumferential friction stress, which generates a torque that causes the twist of the elements on the polymer sheet. Based on the above analysis, a new analytical model of twist angle was proposed according to the law of energy conservation.

To simplify the calculation, as Eq. (19), the assumption of proportional loading was adopted in this study, and the element in the contact zone between tool and polymer sheet was selected as the analysis object. As shown in the Fig. 7, the mass of the element was assumed to be m_{flow}.

$$\frac{\tau_\theta}{\sigma_t'}=\frac{d\gamma_\theta}{d\varepsilon_t}=\frac{\gamma_\theta}{\varepsilon_t}=\frac{\beta}{\ln\cos\alpha}=\text{const} \tag{19}$$

where,

$$\sigma_t'=\sigma_t-\sigma_m=\sigma_t-\frac{1}{3}(\sigma_t+\sigma_\theta+\sigma_\varphi) \tag{20}$$

According to the principle of conservation of energy and combining the above equations, the following equation of twist angleβ' was obtained.

$$\int^S T\beta' dS+\frac{1}{2}m_{flow}v^2=\int^V \tau_\theta\gamma_\theta dV \tag{21}$$

$$\frac{\mu_\theta l_\varphi}{2}d\sigma_t\beta l_\varphi t+\frac{1}{2}V_f\rho v^2=\frac{\beta'}{\ln\cos\alpha}\left(-\frac{1}{\sqrt{3}}\overline{\sigma}\right)\gamma l_\varphi l_\varphi t$$

$$\beta'^2-\frac{2t_0r_t\sin\alpha\mu_\theta(\ln\cos\alpha+n)+2.5{t_0}^2\sin2\alpha n\mu_\theta}{r_t(r_t+2.5t_0\cos\alpha)^2}\beta'+\frac{\sqrt{3}V_f\rho v^2\ln\cos\alpha}{2l_\varphi l_\varphi t\overline{\sigma}}=0$$

$$\beta'=\frac{2t_0r_t\sin\alpha\mu_\theta(\ln\cos\alpha+n)+2.5{t_0}^2\sin2\alpha n\mu_\theta}{2r_t(r_t+2.5t_0\cos\alpha)^2}-\frac{1}{2}\sqrt{\left(\frac{2t_0r_t\sin\alpha\mu_\theta(\ln\cos\alpha+n)+2.5{t_0}^2\sin2\alpha n\mu_\theta}{r_t(r_t+2.5t_0\cos\alpha)^2}\right)^2-\frac{2\sqrt{3}V_f\rho v^2\ln\cos\alpha}{l_\varphi l_\varphi t\overline{\sigma}}} \tag{22}$$

where T is the torque due to tool rotation, m_{flow} is the mass of material flow unit, v is the feed rate, l_φ length and width of element. Eq. (22) shows the twist angle of small element in contact zone between tool and polymer sheet, the twist angle β of formed part could be accumulated by the deformation of each small element in the process of tool sliding, and β can be calculated as ,

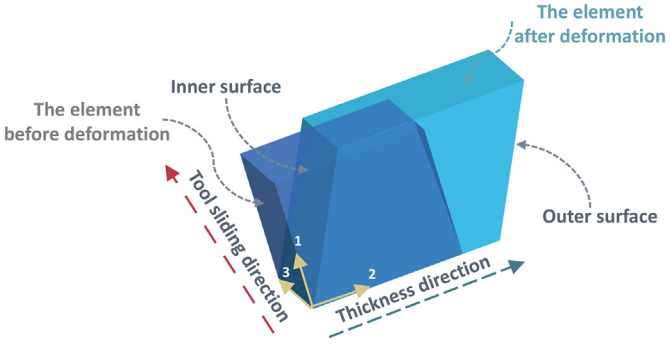

Fig. 6. The deformed element in SPIF of polymer sheet.

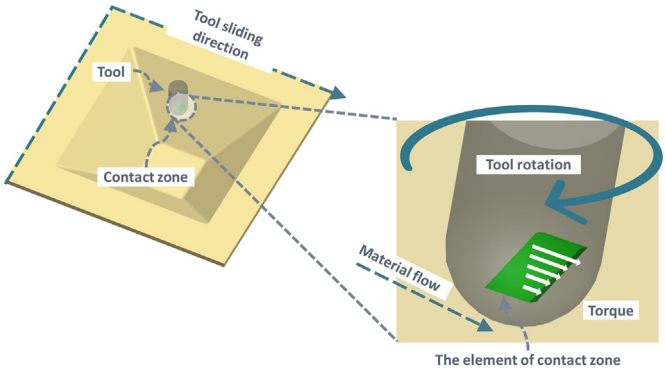

Fig. 7. Torsion mechanism of the element.

$$\beta = \int_0^L \beta' \mathrm{d}\Delta L \tag{23}$$

where L is the tool sliding distance along the trajectory, which can be calculated by feed rate and forming time.

2.2.4. Experimental verifications

In the previous section, twist phenomenon was analyzed from two aspects, the area of material in contact zone pushed by tool along the sliding direction and the strain due to the through thickness stress. In this section, the rationality of inference was verified by experiments. As shown in Fig. 8, the grid was printed on the polymer sheet surface to observe the strain of the formed part. Under the same process parameters as before, it is easy to observe that the grid was deformed along the tool sliding direction, which demonstrated the shear strain caused by friction as described in Section 2.2.2. As Malhotra et al.[25] mentioned, the shear strain is different in the thickness direction. Fig. 8 also describes the distribution of shear strain in the thickness direction, the sliding of tool along the unidirectional trajectory results in the strain imbalance of internal and external surface. With the accumulation of strain, the grid was deformed along the tool sliding direction.

To verify the influence of tool sliding on thickness distribution of formed part, 3D scanning technology was employed to measure the thickness of PEEK formed part, the nephogram of thickness and the variation thickness on the center cross-section with the formed depth are shown in Fig. 9. As mentioned in Section 2.2.1, the thickness distribution of formed parts is asymmetric in the tool movement direction, it means that the polymer sheet has a non-uniform strain field under the unidirectional sliding of the tool, which confirms the flow of material along the tool sliding direction. It can be seen from the thickness distribution diagram of center cross-section that the strain in thickness direction causes the wall thickness change of formed part. As mentioned by Hussain et al. [26], the thickness distribution approximately conforms to the cosine law.

To validate the developed analytical model of twist angle, truncated pyramid part was formed with different wall angles. Fig. 10 shows the comparisons between the calculated and measured twist angles under different forming wall angles, indicating that the twist angle increases with the increase of forming wall angle, which agrees well with the experimental values. As shown in the figure, although the analytical model can predict the trend of twist angle, there is still some difference between the calculated value and the measured value. The most likely causes of the deviations are mainly due to that the flow material volume of polymer sheet was simplified to some extent, and the influence of micro mechanism and process parameters on material flow stress has not been fully considered.

In summary, the unidirectional trajectory strategy is the main factor that caused twist of formed part in SPIF. Because the tool moves in one direction, strain and sheet material flow of formed part in tool movement direction are asymmetric, with the increase of the wall angle, the asymmetry becomes more intense, which eventually leads to twist phenomena in SPIF, even seriously affects the geometric accuracy of formed part.

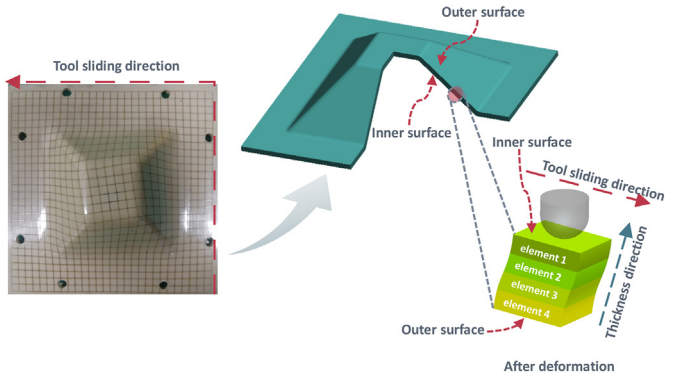

Fig. 8. Tangential strain of formed part.

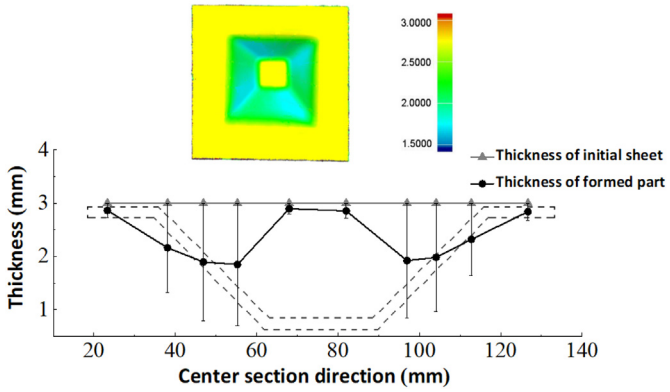

Fig. 9. Thickness distribution diagram of the formed part.

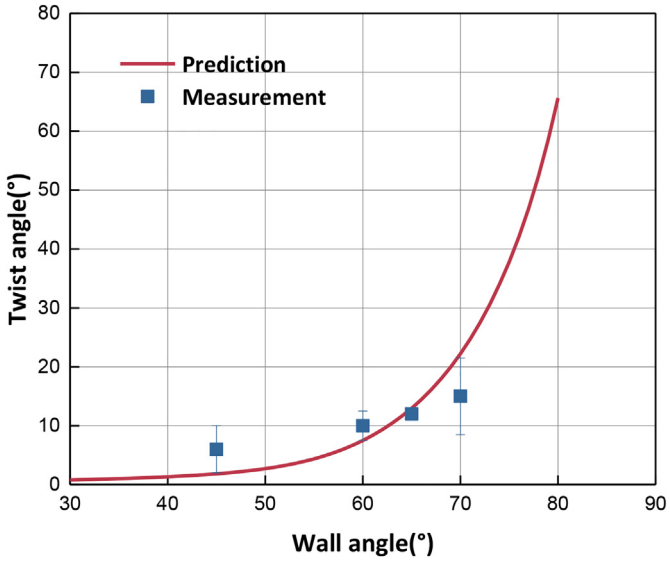

Fig. 10. Variations of twist angle under different wall angles.

3. A novel alternative spiral trajectory

According to the analysis and experiments on mechanisms of polymer thermally assisted SPIF, it is commonly recognized that unidirectional trajectory can easily causes material to flow along tool sliding direction in the contact zone, and through thickness stress causes accumulation effect of shear strain in tool sliding direction. In other words, twist phenomena are inevitable in such a condition. To counteract the unidirectional flow and strain accumulation effect of polymer sheet, further improve the geometric accuracy of formed part by SPIF, a novel alternative spiral trajectory strategy was proposed, which was compared with the unidirectional trajectory. The superiority of alternative trajectory was also confirmed.

3.1. Trajectory generation algorithm

Matsubara et al. [27] believed that accumulation effect can be prevented by changing the tool trajectory direction. However, the

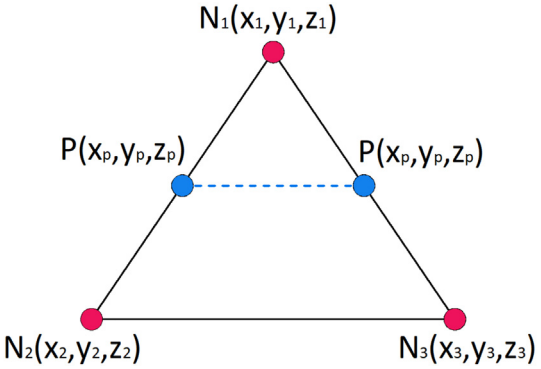

Fig. 11. Interpolation of contour.

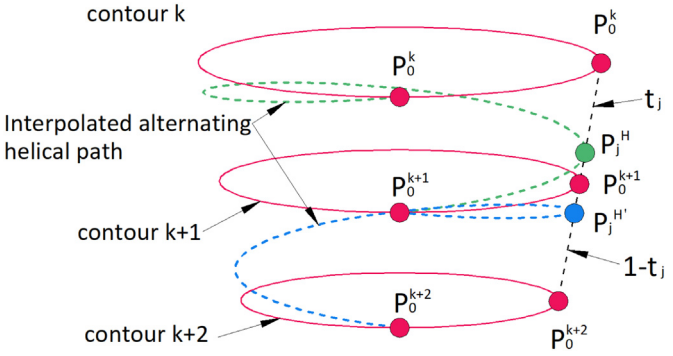

Fig. 13. Linear interpolation alternate trajectory of three adjacent contour lines.

traditional alternate trajectory was composed of continuous 2D contour, which was separated by discrete step depth in the depth direction, resulting in stress concentration and surface quality degradation at the contour transition point. Therefore, a continuous 3D tool trajectory was generated based on spiral trajectory. Durante et al. [13] proposed to generate alternate trajectory with a fixed height drop on the side wall of pyramid-shaped, and preliminarily verified that alternate trajectory can improve formability and reduce twist phenomena of PC part compared with unidirectional trajectory. In this study, trajectory generation strategy was proposed based on the following principles:

(1) The contour lines were generated by interpolation of specified height on STL model;
(2) The final alternate spiral trajectory was generated by the linear interpolation of two neighboring contour lines.

As shown in Fig. 11, if the specified height z_p and three points N_1, N_2, N_3 of any triangular face on the STL model follows the relationship: $z_1<z_p$, $z_2>z_p$, $z_3>z_p$, the contour can be calculated by the intersection of N_1N_2 and N_1N_3. Calculating the contour lines with step depth of 0.4mm, the calculated contour lines are shown in Fig. 12.

Based on the linear interpolation of three neighboring contour lines, the tool trajectory of clockwise and counterclockwise were successively generated, the final tool trajectory is shown in Fig. 13, and the points on the trajectory can be obtained by Eq. (24),

$$\begin{cases} x_j^H = \dfrac{t_j-1}{0-1}x_i^k + \dfrac{t_j-0}{1-0}x_i^{k+1} \\ y_j^H = (-1)^k\left\langle \dfrac{t_j-1}{0-1}y_i^k + \dfrac{t_j-0}{1-0}y_i^{k+1} \right\rangle \\ z_j^H = \dfrac{t_j-1}{0-1}z_i^k + \dfrac{t_j-0}{1-0}z_i^{k+1} \end{cases} \tag{24}$$

simplify as:

$$\begin{cases} x_j^H = t_j x_i^{k+1} - (t_j-1)x_i^k \\ y_j^H = (-1)^k\left\langle t_j y_i^{k+1} - (t_j-1)y_i^k \right\rangle \\ z_j^H = t_j z_i^{k+1} - (t_j-1)z_i^k \end{cases} \tag{25}$$

where $\sum|x_{i+1}^k - x_i^k| / \sum|x_{i+1}^k - x_i^k|$ is the point on the spiral path, $\langle x_j^H, y_j^H, z_j^H\rangle$ is the coordinate of point P_j^H on alternate trajectory. $\langle x_j^k, y_j^k, z_j^k\rangle$ is the coordinate of point P^k on the k^{th} contour line. $\langle x_j^{k+1}, y_j^{k+1}, z_j^{k+1}\rangle$ is the coordinate of point P^{k+1} on the $(k+1)^{th}$ contour line. $\langle x_j^{k+2}, y_j^{k+2}, z_j^{k+2}\rangle$ is the coordinate of point P^{k+2}on the $(k+2)^{th}$ contour line. j is the total number of points calculated, and N is the number of points on contour lines.

As Lu et al. [28] mentioned, the contour density corresponding to different incremental depth affects the surface roughness of formed part. The scallop height is the main factor affecting the surface roughness. Therefore, the scallop height of alternate spiral trajectory was calculated. As shown in Fig. 13, the distance of two neighboring contour lines in depth direction is not constant. This effect can be described by fluctuation in a certain range. The maximum value of scallop height is approximately calculated by $2\Delta z$, and the minimum value of scallop height is approximately calculated byΔz. According to Fig. 14, the geometric relationship between step depth Δz and scallop height was established as follows,

$$r^2 = (r-s)^2 + \left(\frac{\Delta z}{2\sin\alpha}\right)^2 \tag{26}$$

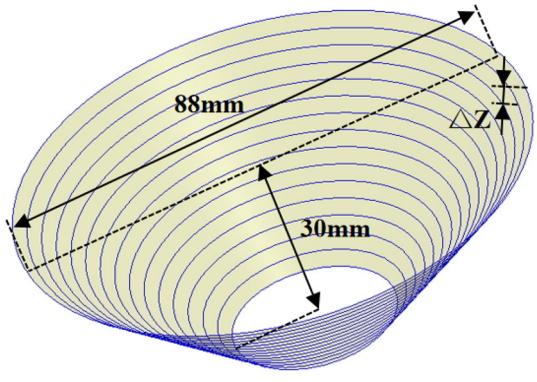

Fig. 12. Contour of constant step depth.

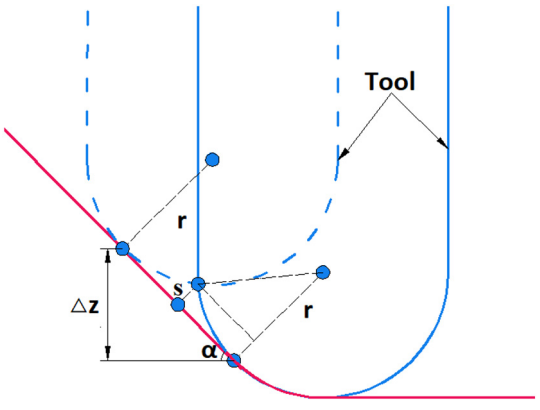

Fig. 14. Relationship between step depth and scallop height.

simplified as,

$$s = r - \sqrt{r^2 - \left(\frac{\Delta z}{2\ \sin\alpha}\right)^2} \tag{27}$$

So, the scallop height between maximum value and minimum value, as expression (28),

$$r - \sqrt{r^2 - \left(\frac{\Delta z}{2\ \sin\alpha}\right)^2} < s < r - \sqrt{r^2 - \left(\frac{\Delta z}{\sin a}\right)^2} \tag{28}$$

It can be seen from the expression that the scallop height is affected by step depth, tool diameter and wall angle. As shown in Fig. 15, the scallop height decreases with the decrease of step depth, tool diameter and wall angle, so the surface roughness and the forming time of formed part can be reduced by selecting reasonable parameters.

3.2. Experimental verification

For the unidirectional trajectory, each element is deformed in the same direction under tool sliding, so accumulation effect cannot be eliminated. As shown in Section 2.2.3, the twist angle of the formed part is eventually caused by the accumulation of each element torsion. The alternative trajectory can overcome this disadvantage of unidirectional trajectory. The advantage of alternative trajectory is that the tool alternative sliding can counteract the accumulation of twist phenomena. To this end, two adjacent movements of the tool are in opposite directions, so the element torsion caused by tool sliding in previous revolution could be significantly eliminated due to the change of the tool sliding direction in the next revolution, the principle is shown in Eq. (29).

$$\beta = \int^{L_1} \beta' \mathrm{d}\Delta l - \int^{L_2} \beta' \mathrm{d}\Delta l + \int^{L_3} \beta' \mathrm{d}\Delta l - \cdots \int^{L_N} \beta' \mathrm{d}\Delta l \tag{29}$$

As shown in Fig. 16, due to the change of wall angle, the reverse movement of the tool does not completely counteract the torsion caused by the previous turn, unless the wall angle is 90°. It is possible to reduce the numerical difference of twist angle caused by the forward and reverse movement of the tool by reducing the step depth. According to the experimental results shown in Fig. 17(b), the final twist angle could be acceptable because the value is less than 1°. The geometric accuracy is not greatly affected by such a small twist angle.

As shown in Fig. 3, twist phenomenon was found in pyramid formed part of PEEK. Therefore, the 70° pyramid part was formed by using the developed alternate spiral trajectory. Combined with above calculation of scallop height, the reasonable process parameters could be fixed as follows: the incremental depth of 0.4mm, the tool diameter of 10 mm, the tool rotation speed of 100 r/min and the feed rate of 1000 mm/min.

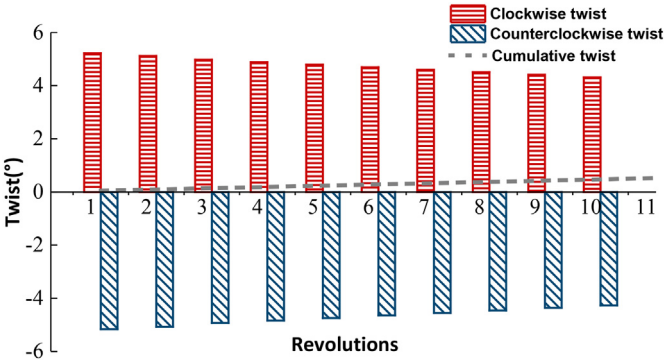

Fig. 16. Twist angle of the first ten revolutions.

As shown in Fig. 17, compared with the unidirectional trajectory, the twist angle of PEEK formed part was almost eliminated by the alternate spiral trajectory, due to the tool reverse sliding along two adjacent trajectory lines, the material flow and strain accumulation were significantly counteracted in the opposite direction, therefore, the materials of formed part could be symmetrically distributed. The experimental

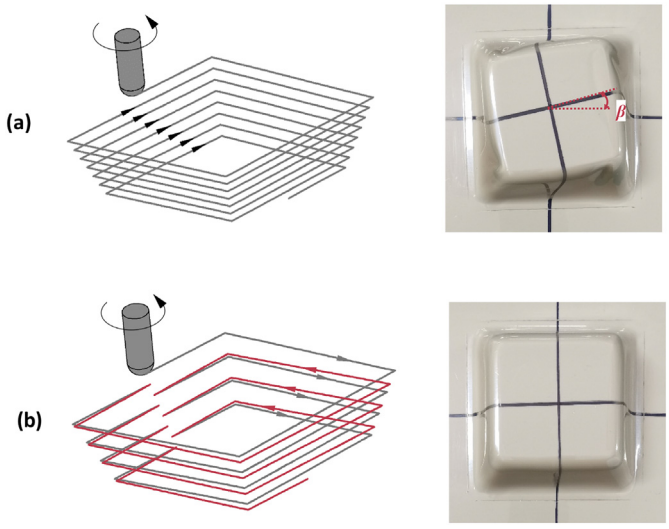

Fig. 17. Comparison of (a) unidirectional trajectory and (b) alternate trajectory.

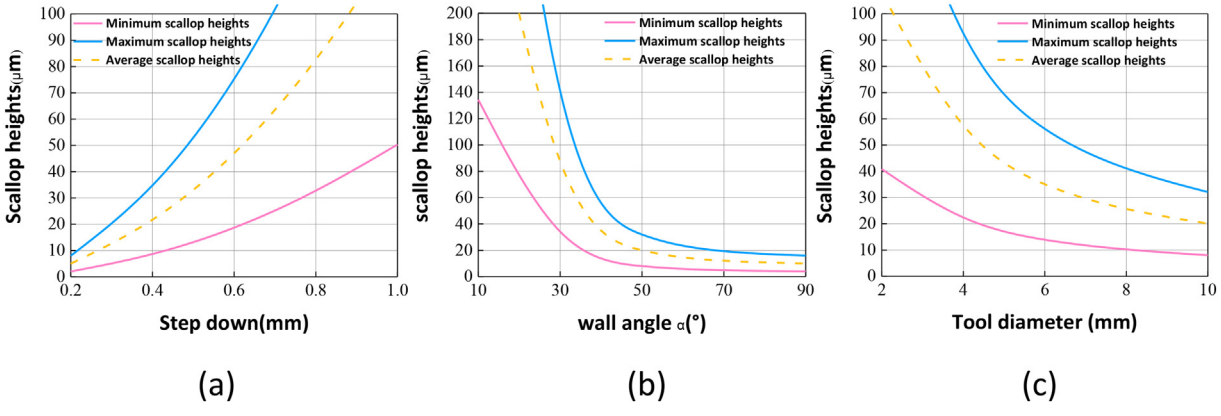

Fig. 15. Influence of (a) step depth, (b) wall angle and (c) tool diameter on the scallop height.

comparison results demonstrated the reliability of mechanism analysis and also verified the superiority of the developed alternate trajectory.

4. The applicability of the trajectory and discussions

4.1. SPIF of PVC by alternative trajectory

The alternate trajectory developed in this study could significantly increase the geometry accuracy of formed part: the twist and wrinkle could be greatly reduced. To further verify the applicability of the developed trajectory, SPIF experiments of PVC were carried out. Table 2 gives the mechanical and thermal properties of the material.

As described by Franzen et al. [3], three failure modes of PVC were revealed in single point increment forming, which has a great effect on the geometric accuracy and formability of formed part. As for fracture, a certain proportion of cracks in parts mainly occurred when the forming temperature is close to the glass transition temperature. In this study, the thermal assisted incremental forming setup was developed to improve the formability of the polymer sheet in SPIF. As shown in Fig. 18, for the formed part with wall angle of 70°, the twist angle increases significantly, and serious wrinkle occurs along the direction of tool sliding. For pyramid part, wrinkle is obviously found at the corners of formed part as shown in Fig. 18(a). While for the truncated cone part, the wrinkle is also found on the entire formed surface of part as shown in Fig. 18(b). The torsion of polymer sheet element in the contact zone has not been compensated under the continuous unidirectional spiral trajectory, which strengthens the final torsion effect. The accumulated torsion along the tool sliding direction causes the rotation of formed part around the central axis, resulting in wrinkle. The experimental results show that with the increase of the forming wall angle, the wrinkle phenomenon increases significantly. This is consistent with the failure mode proposed by Franzen et al. [3].

To verify the effect of the alternate trajectory on twist phenomena, two different forming trajectories were compared and the experimental results are shown in Fig. 19. From the Fig. 19, the alternate trajectory can significantly eliminate the twist and wrinkle at transition edge of the pyramid formed part. For conical parts, the continuous torsion around the central axis is also completely eliminated.

In summary, twist accumulation of polymer sheet under the action of tool sliding can be effectively eliminated by alternate spiral path. The alternate movement of the tool can offset the twist angle generated in the previous turn, and finally eliminate the twist.

4.2. The difference of twist mechanism in SPIF of metal and polymer

The twist mechanism in SPIF of metal material was firstly clarified by Duflou et al. [11]. It is commonly recognized that the twist phenomena could be divided into forward twist with low wall angle and reverse twist with high wall angle. Similar experimental results were also found in the following work by Change and Chen [23] in SPIF of aluminum alloy sheet.

The twist of polymer is more severe than that of metal due to the macromolecular structure and mechanical properties of polymeric materials. This phenomena have been verified by Durante et al. [13] who found that the twist angle is higher than 20° when unidirectional trajectory was employed. Similar experimental results were also found in our previous work [15].

The difference of twist phenomena in SPIF of metal and polymer may be explained by the following reasons. When the tool moves along the trajectory, the meridional force is greater than the circumferential force caused by the through thickness shear. In the process of incremental sheet forming, the deformation is mainly due to the action of meridional force. As for metal sheet, the circumferential force is always not enough to result in much material deformation along tool sliding direction. However, as for polymer sheet, especially in the heating conditions, the circumferential force could push much more polymeric materials to be deformed even flow along the tool sliding direction, which eventually plays a key role in accumulation of twist defect. This is the primary reason why the kinetic energy of the flow polymeric

Table 2
Material properties of PVC.

Mechanical properties		Thermal properties	
Elastic modulus (GPa)	2.9-3.4	Thermal conductivity (W/mk)	0.16
Density (kg/m^3)	1380	Specific heat (J/kg K)	900
Poisso's ratio	0.38	Glass transition temperature(K)	361
Yield stress (MPa)	50-80	Melting temperature(K)	486

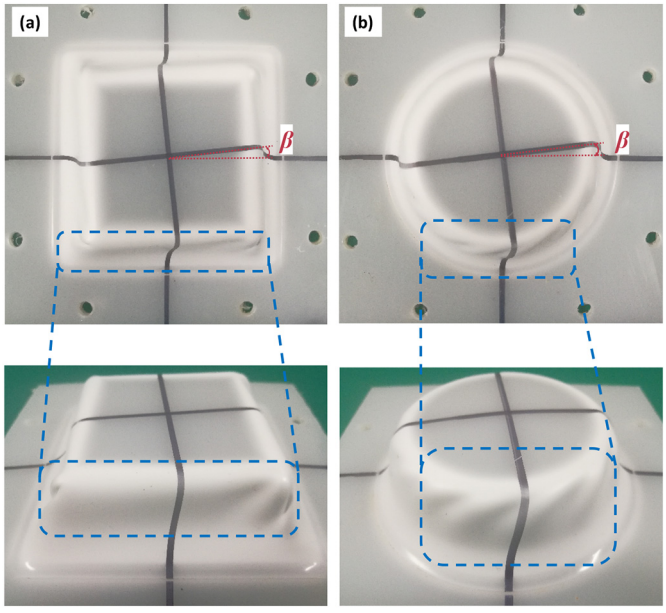

Fig. 18. The formed (a) pyramid part and (b) truncated cone part of PVC by using of the unidirectional toolpath.

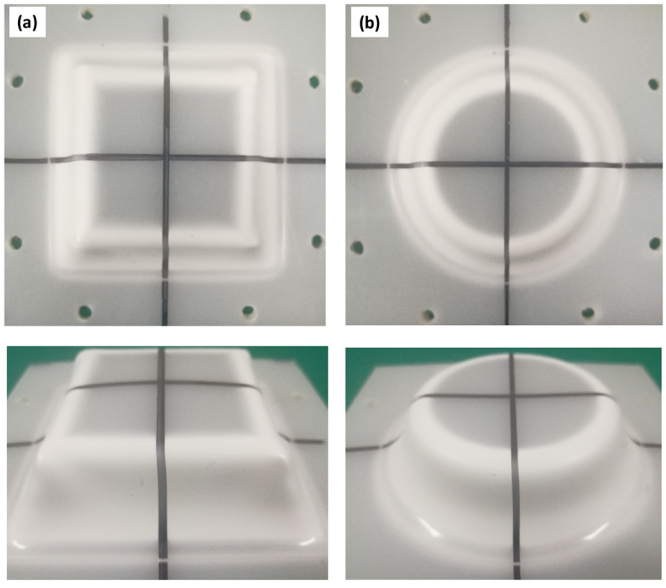

Fig. 19. The formed (a) pyramid part and (b) truncated cone part of PVC by using the alternate toolpath.

material volume was considered in Eq. (21). Meanwhile, the change of twist direction controlled by the circumferential force is not obvious in the heat-assisted SPIF of thermoplastic polymer.

In summary, the twist is a critical factor that affects the geometric accuracy of formed part in incremental forming. To eliminate the failure mode of thermoplastic polymer, as the first step, the self-developed thermal assisted incremental forming setup was developed to reduce the probability of fracture and further improve the formability of polymer sheet. To this end, polymer sheet was heated to close to the glass transition temperature, which effectively enhances the ductility of polymer sheet. Second, by use of alternate trajectory, the polymer sheet twist phenomena were effectually restrained.

5. Conclusions

(1) A new theoretical model was proposed to calculate the twist angle during SPIF of polymer. Through compared the SPIF experiment results, it is demonstrated that the developed model has fine predicting precision.
(2) The experimental results show that material flow and shear strain always accumulate along the direction of tool movement, which eventually leads to the thickness asymmetric distribution of the formed part. It is confirmed that the twist and wrinkle are inevitable by using unidirectional trajectory. Case studies also verified that the thickness of formed parts conforms to cosine theorem in depth direction.
(3) Based on the influence of unidirectional trajectory on twist and wrinkle in the process of polymer thermal assisted single point incremental forming, a novel alternative spiral trajectory algorithm was proposed. The alternative trajectory was generated by used the interpolation algorithm between three neighbouring contour lines, and the comparison shows that the novel alternate trajectory can greatly improve the geometry accuracy of the formed parts.

Declaration of Competing Interest

The authors declare that they have no known competing financial interests or personal relationships that could have appeared to influence the work reported in this paper.

Acknowledgements

This work was funded by the Shanghai Pujiang Program (18PJD019) and Program of Shanghai Academic Research Leader (19XD1401900).

References

[1] P.A.F. Martins, N. Bay, M. Skjoedt, M.B. Silva, Theory of single point incremental forming, CIRP Ann. Manufact. Technol. 57 (2008) 247–252, https://doi.org/10.1016/j.cirp.2008.03.047.
[2] J.R. Duflou, A.-M. Habraken, J. Cao, R. Malhotra, M. Bambach, D. Adams, H. Vanhove, A. Mohammadi, J. Jeswiet, Single point incremental forming: state-of-the-art and products, Int. J. Mater. Form 11 (2018) 743–773, https://doi.org/10.1007/s12289-017-1387-y.
[3] V. Franzen, L. Kwiatkowski, P.A.F. Martins, A.E. Tekkaya, Single point incremental forming of PVC, J. Mater. Process. Technol. 209 (2008) 462–469, https://doi.org/10.1016/j.jmatprotec.2008.02.013.
[4] P.A.F. Martins, L. Kwiatkowski, V. Franzen, A.E. Tekkaya, M. Kleiner, Single point incremental forming of polymers, CIRP Ann. Manuf. Tehnol. 58 (2009) 229–232, https://doi.org/10.1016/j.cirp.2009.03.095.
[5] M.B. Silva, L.M. Alves, P.A.F. Martins, Single point incremental forming of PVC: experimental findings and theoretical interpretation, Eur. J. Mech. A Solid 29 (2010) 557–566, https://doi.org/10.1016/j.euromechsol.2010.03.008.
[6] M.B. Silva, M. Skjoedt, P.A.F. Martins, N. Bay, Revisiting the fundamentals of single point incremental forming by means of membrane analysis, Int. J. Mach. Tool Manuf. 48 (2008) 73–83, https://doi.org/10.1016/j.ijmachtools.2007.07.004.
[7] T.A. Marques, M.B. Silva, P.A.F. Martins, On the potential of single point incremental forming of sheet polymer parts, Int. J. Adv. Manf. Technol. 60 (2012) 75–86, https://doi.org/10.1007/s00170-011-3585-y.
[8] S. Matsubara, A computer numerically controlled dieless incremental forming of a sheet metal, Proc. Inst. Mech. Eng. B-J. Eng 215 (2001) 959–966, https://doi.org/10.1243/0954405011518863.
[9] J. Jeswiet, F. Micari, G. Hirt, A. Bramley, J.R. Duflou, J. Allwood, Asymmetric single point incremental forming of sheet metal, CIRP Ann. Manuf. Technol 54 (2005) 623–650, https://doi.org/10.1016/S0007-8506 (07) 60021-3.
[10] H. Vanhove, J. Verbert, J. Gu, I. Vasilakos, J.R. Duflou, An experimental study of twist phenomena in single point incremental forming, Int. J. Mater. Form. 3 (2010) 975–978, https://doi.org/10.1007/s12289-010-0932-8.
[11] J.R. Duflou, H. Vanhove, J. Verbert, J. Gu, I. Vasilakos, P. Eyckens, Twist revisited: twist phenomena in single point incremental forming, CIRP Ann. Manuf. Tehnol. 59 (2010) 307–310, https://doi.org/10.1016/j.cirp.2010.03.018.
[12] S. Dejardin, J.C. Gelin, S. Thibaud, Experimental investigations and numerical analysis for improving knowledge of incremental sheet forming process for sheet metal parts, J. Mater. Process. Technol. 210 (2010) 363–369, https://doi.org/10.1016/j.jmatprotec.2009.09.025.
[13] M. Durante, A. Formisano, F. Lambiase, Incremental forming of polycarbonate sheets, J. Mater. Process. Tech. 253 (2018) 57–63, https://doi.org/10.1016/j.jmatprotec.2017.11.005.
[14] Z.D. Chang, J. Chen, Mechanism of the twist in incremental sheet forming process, J. Mater. Process. Tech. 276 (2020) 116396, https://doi.org/10.1016/j.jmatprotec.2017.11.005.
[15] Z.Y. Yang, F. Chen, S. Gatea, H. Ou, Design of the novel hot incremental sheet forming experimental setup, characterization of formability behavior of polyether-ether-ketone (PEEK), Int. J. Adv. Manuf. Techol. 106 (2020) 5365–5381, https://doi.org/10.1007/s00170-020-05035-0.
[16] S. Matsubara, A computer numerically controlled dieless incremental forming of a sheet metal, P. I. Mech. Eng. B-J. Eng. 215 (2001) 959–966, https://doi.org/10.1243/0954405011518863.
[17] P.A.F. Martins, L. Kwiatkowski, V. Franzen, A.E. Tekkaya, M. Kleiner, Single point incremental forming of polymers, CIRP Ann. Manuf. Tehnol. 58 (2009) 229–232, https://doi.org/10.1016/j.cirp.2009.03.095.
[18] F. Chen, H. Ou, S. Gatea, H. Long, Hot tensile fracture characteristics and constitutive modelling of polyether-ether-ketone (PEEK), Polymer Test. 63 (2017) 168–179, https://doi.org/10.1016/j.polymertesting.2017.07.032.
[19] A.R. McLauchlin, O.R. Ghita, L. Savage, Studies on the reprocessability of poly (ether ether ketone) (PEEK), J. Mater. Process. Tech 214 (2014) 75–80, https://doi.org/10.1016/j.jmatprotec.2013.07.010.
[20] J. Asghar, R. Lingam, E. Shibin, N.V. Reddy, Tool path design for enhancement of accuracy in single-point incremental forming, P. I. Mech. Eng. B, J. Eng 228 (2014) 1027–1035, https://doi.org/10.1177/0954405413512812.
[21] Y. Li, W.J.T. Daniel, Z. Liu, H. Lu, P.A. Meehan, Deformation mechanics and efficient force prediction in single point incremental forming, J. Mater. Process. Tech. 221 (2015) 100–111, https://doi.org/10.1016/j.jmatprotec.2015.02.009.
[22] F.Y. Liu, X.Q. Li, Y.L. Li, Z.J. Wang, W.D. Zhai, F.Y. Li, J.F. Li, Modelling of the effects of process parameters on energy consumption for incremental sheet forming process, J Clean Prod. 250 (2020) 119456, https://doi.org/10.1016/j.jclepro.2019.119456.
[23] Z.D. Chang, M, Li, J, Chen. Analytical modeling and experimental validation of the forming force in several typical incremental sheet forming processes. Int. J. Mach. Tool Manuf. 140 (2019) 62–76, https://doi.org/10.1016/j.ijmachtools.2019.03.003.
[24] K. Jackson, J. Allwood, The mechanics of incremental sheet forming, J. Mater. Process. Technol. 209 (2009) 1158–1174, https://doi.org/10.1016/j.jmatprotec.2008.03.025.
[25] R. Malhotra, L. Xue, T. Belytschko, J. Cao, Mechanics of fracture in single point incremental forming, J. Mater. Process. Technol 212 (2012) 1573–1590, https://doi.org/10.1016/j.jmatprotec.2012.02.021.
[26] G. Hussain, L. Gao, A novel method to test the thinning limits of sheet metals in negative incremental forming, Int. J. Mach. Tools Manuf. 47 (2007) 419–435, https://doi.org/10.1016/j.ijmachtools.2006.06.015.
[27] S. Matsubara, A Computer numerically controlled dieless incremental forming of a sheet metal, J. Eng. Mech. 215 (2001) 959–966, https://doi.org/10.1243/0954405011518863.
[28] B. Lu, J. Chen, H. Ou, J. Cao, Feature-based tool path generation approach for incremental sheet forming process, J. Mater. Process. Technol. 213 (2013) 1221–1233, https://doi.org/10.1016/j.jmatprotec.2013.01.023.